

Overstability of Plasma Slow Electron Holes

I H Hutchinson

Plasma Science and Fusion Center, Massachusetts Institute of Technology, Cambridge,
MA, USA

December 9, 2021

Abstract

Sufficient conditions are found on the ion velocity distribution f_i and potential amplitude for stability of steady electron holes moving at slow speeds, coinciding with the bulk of f_i . Fully establishing stability requires calculation of the ion response to shift potential perturbations having an entire range of oscillatory frequencies, because under some conditions real frequencies intermediate between the ion and electron responses prove to be unstable even when the extremes are not. The mechanism of this overstability is explained and calculated in detail. Electron holes of peak potential ψ less than approximately 0.01 times the background temperature ($\psi \lesssim 0.01T_0/e$) avoid the oscillatory instability entirely. For them, the *necessary* condition that there be a local minimum in f_i in which the hole resides is also *sufficient*, unless the magnetic field B is low enough to permit the transverse instability having finite wavenumber k perpendicular to B .

1 Introduction

Plasma electron holes are solitary positive potential structures, sustained by a deficit of collisionless electrons on trapped phase-space orbits [1]. Most often, the velocity v_h of the frame in which the hole is steady moves much faster along the magnetic field than typical ion velocities, with the result that ion perturbation can be ignored. An extensive list of references to satellite measurements of holes in various space regions is given in the introduction of [2]. However, *slow electron holes*, defined as those for which there is a significant ion population traveling at zero speed in the hole's rest frame, have also recently been detected by satellite measurements in space plasmas [2–5]. Past simulations have almost always shown that slow holes do not *remain* slow, but are accelerated by repulsion from the associated ion perturbation [6–10] until they are fast, that is, their speed in the ion frame greatly exceeds the ion velocity spread, and ion interaction has virtually stopped. This poses a puzzle as to how slow electron holes can remain slow, as they sometimes seem to do in nature.

That puzzle has recently been solved by showing that, although single-humped ion velocity distributions always lead to the self-acceleration instability, if a local minimum exists in the distribution function $f_i(v)$, in which the hole velocity v_h lies, then the ion force on

the hole reverses sign and becomes an effective attraction [11]. Moreover, in satellite measurements, when slow holes are present, the background ion distributions are observed to have just this feature: a local minimum at the hole velocity [5]. Thus theory says that a necessary condition for stability is that a local minimum in f_i is present; and in experiments this condition is satisfied.

What has not previously been shown theoretically, because the prior analysis [11] was essentially quasi-static, is whether there are instabilities with non-zero real frequency (a situation sometimes called overstability) remaining even if the local minimum condition is satisfied. This is a significant concern, because it is known that when an electron hole's velocity is within a few ion sound speeds of even a narrow-velocity-spread ion distribution whose phase-space density is negligible at the hole speed v_h , there are oscillatory instabilities in hole velocity [12, 13]. Moreover unpublished PIC simulations (by the present author) of fully self-consistent slow electron holes initialized in the presence of local f_i minimum have shown slowly growing velocity oscillations which eventually escape the attractive force of the ion equilibrium charge, and become *fast*.

The present theory therefore extends the previous analysis to a full evaluation of the stability of shift perturbations of arbitrary complex frequency. This requires one to use a fully kinetic formulation of the responses of electrons *and* ions, evaluating the contribution of the entire velocity distributions, abandoning any simplifying beam treatment of the ions. To my knowledge such a full stability analysis has not previously been accomplished. It is achieved by multidimensional numerical integration of the perturbed force over the linearized perturbation solution of the Vlasov equation in an electrostatic approximation.

In section 2 the theoretical formulation and solution of the linearized stability of slow electron holes is described. Section 3 gives one-dimensional stability results for equal ion and electron temperatures, in which the mechanisms and regimes of instability are identified. Section 4 shows how the results are affected by ion temperature, transverse wave-number, and magnetic field strength.

2 Formulation and Solution Method

Unless otherwise indicated, in this paper dimensionless units are used with length normalized to Debye length $\lambda_D = \sqrt{\epsilon_0 T_0 / n_0 q_e^2}$, velocity to electron thermal speeds $v_{te} = \sqrt{T_0 / m_e}$, electric potential to thermal energy T_0 / q_e and frequency to electron plasma frequency $\omega_{pe} = v_{te} / \lambda_D$ (time normalized to ω_{pe}^{-1}). This normalization reduces the one-dimensional electron Vlasov equation to the form

$$\frac{\partial f}{\partial t} + v \frac{\partial f}{\partial z} - q_e \frac{\partial \phi}{\partial z} \frac{\partial f}{\partial v} = 0. \quad (1)$$

The ion Vlasov equation is reduced to exactly the same form by using units in which time is measured instead in terms of $\omega_{pi} = \sqrt{m_e / m_i} \omega_{pe}$, except that instead of $q_e = -1$ the particle charge for ions is simply reversed $q_i = 1$ (so $q\phi$ is the potential *energy*). Ions in this paper all have mass $m_i = 1836m_e$; they are protons.

The formulation and analysis of the electron response follows closely the treatment of previous papers [14–16], which should be consulted for the mathematical derivation. Only an

outline description of the method is given here (thus glossing over a large amount of algebraic and numerical work). Vlasov's equation can be integrated along the equilibrium (zeroth order) orbits to obtain the first-order perturbation to the distribution function f_1 caused by a first-order electric potential perturbation (relative to the non-uniform hole equilibrium)

$$\phi_1(\mathbf{x}, t) = \hat{\phi}(z) \exp i(ky - \omega t), \quad (2)$$

(including a perturbation transverse wave vector in the y -direction, which for the first three sections of the paper will simply be $k = 0$, i.e. one-dimensional variation along the applied uniform magnetic field direction z). The integration along unperturbed helical orbits leads to an expansion in (integer m) harmonics $\omega_m = m\Omega + \omega$ of the cyclotron frequency ($\Omega = eB/m_e$, which represents the magnetic field strength), in which the potential orbit-integrated over earlier time is

$$\Phi_m(z, t) \equiv \int_{-\infty}^t \hat{\phi}(z(\tau)) e^{-i\omega_m(\tau-t)} d\tau, \quad (3)$$

where $z(\tau) = z(t) + \int_t^\tau v_z(t') dt'$ is the orbit position at earlier time τ . For positive imaginary part of ω the integrals converge and the perturbation in the parallel distribution function (integrated over Maxwellian transverse velocities) then can be found as [see 14, eq:5.9]

$$f_{e\parallel 1}(y, t) = q_e \phi_1(t) \left. \frac{\partial f_{e\parallel 0}}{\partial W_{e\parallel}} \right|_t + \sum_{m=-\infty}^{\infty} i \left[\omega_m \frac{\partial f_{e\parallel 0}}{\partial W_{e\parallel}} + (\omega_m - \omega) \frac{f_{e\parallel 0}}{T_\perp} \right] q_e \Phi_m e^{-\zeta_t^2} I_m(\zeta_t^2) e^{i(ky - \omega t)}, \quad (4)$$

where q_e is electron charge ($= -1$ in non-dimensionalized units), $W_{e\parallel}$ is the parallel energy $\frac{1}{2}v_z^2 + q_e\phi$ (m_e being unity), $f_{e\parallel 0}$ is the unperturbed parallel distribution function, a function only of energy, and T_\perp is the perpendicular temperature. The parameter ζ_t is the transverse wavenumber k times the thermal Larmor radius, so that $\zeta_t^2 = k^2 T_\perp / \Omega^2$, and I_m is the modified Bessel function. When ζ_t is small, e.g. because k is small (zero even) or Ω is large, then the small-argument Bessel function behavior ($I_m(\xi) \rightarrow (\xi/2)^m / \Gamma(m+1)$) implies that only the $m = 0$ cyclotron harmonic is non-negligible. It corresponds to a one-dimensional motion treatment.

The first term of eq. (4) is the ‘‘adiabatic’’ perturbation that would arise from a steady potential difference. It does not contribute to the needed response. The remaining harmonic sum is the non-adiabatic contribution denoted $\tilde{f}_{e\parallel}$.

A key formal difficulty is to find the shape of the linearized eigenfunction $\hat{\phi}(z)$ which self-consistently satisfies the Vlasov and Poisson equations; this is an integro-differential eigenproblem. For slow time dependence relative to particle transit time, it can be argued on general grounds that the eigenmode consists of a spatial shift (by small distance ξ independent of position) of the equilibrium potential profile (ϕ_0) [see 14, section 3.1] giving:

$$\hat{\phi} = -\xi \frac{\partial \phi_0}{\partial z}, \quad (5)$$

which is the perturbation we analyze. Although this is only an approximation to the exact eigenmode, the corresponding eigenvalue of our system can be found to next order accuracy by using a ‘‘Rayleigh Quotient’’ variational approximation [see e.g. 17]. This mathematical procedure is equivalent to requiring the total force exerted on the particles by the electrostatic

field under the influence of the assumed shift eigenmode to equal zero (or to balance the transverse momentum transfer by Maxwell stress if $k \neq 0$, [see 14, section 3]). It is the kinematic momentum balance of the electron hole regarded as a rigid composite object. Suppressing the linear ξ factor, the force on the electrons is equal to the force of ϕ_0 on the non-adiabatic perturbed electron density

$$\tilde{F}_e = - \int \frac{d\phi_0}{dz} q_e \left(\int \tilde{f}_{e\parallel} dv_z \right) dz. \quad (6)$$

The transverse Maxwell stress force when $k \neq 0$ is

$$F_E \equiv -k^2 \int \frac{d\phi_0}{dz} \hat{\phi} dz, \quad (7)$$

into which we substitute the shift-mode, eqs. (5 and 2).

The essential departure from the previous analysis, required here for *slow* electron holes, is that the force on the ions cannot be ignored. By the same analysis as the electrons, but substituting ion parameters, that force is

$$\tilde{F}_i = - \int \frac{d\phi_0}{dz} q_i \left(\int \tilde{f}_{i\parallel} dv_z \right) dz, \quad (8)$$

where

$$\tilde{f}_{i\parallel} = \sum_{m=-\infty}^{\infty} i \left[\omega_{im} \frac{\partial f_{i\parallel 0}}{\partial W_{i\parallel}} + (\omega_{im} - \omega) \frac{f_{i\parallel 0}}{T_{i\perp}} \right] q_i \Phi_m e^{-\zeta_{it}^2} I_m(\zeta_{it}^2), \quad (9)$$

with $\Omega_i = (m_e/m_i)\Omega$, $\omega_{im} = \omega + m\Omega_i$, and $\zeta_{it}^2 = k^2 T_{i\perp} / \Omega_i^2$. In practice, it is most convenient to calculate the ion force by the same code as the electron force, except reversing the potential sign (as proxy for charge sign), and using a frequency (ω) scaled to be larger by $\sqrt{m_i/m_e}$. Effectively that amounts to solving the ion perturbation in *ion* scaled units, in which the length scale is the same (using the same reference temperature) and so for the same density we get the same scaled force units.

The specific hole equilibrium potential shape analyzed is chosen to be

$$\phi_0 = \psi \operatorname{sech}^4(z/4). \quad (10)$$

The background (untrapped) electron parallel velocity distribution is taken as an unshifted Maxwellian of temperature T_0 , and $T_{\perp} = T_0$. For uniform equilibrium density of ions, the self-consistent equilibrium *trapped* electron distribution is [16] (for negative $W_{e\parallel}$)

$$f_{t\parallel 0} = f_{e0} \left[\frac{2}{\sqrt{\pi}} \sqrt{-W_{e\parallel}} + \frac{15}{16} \sqrt{\frac{\pi}{\psi}} W_{e\parallel} + \exp(-W_{e\parallel}) \operatorname{erfc}(\sqrt{-W_{e\parallel}}) \right], \quad (11)$$

where f_{e0} is the untrapped electron distribution value at zero energy. It will be shown later that ion equilibrium density nonuniformity gives an adjustment to the trapped electrons, but it is fairly small at relevant ψ for threshold ion distribution shapes.

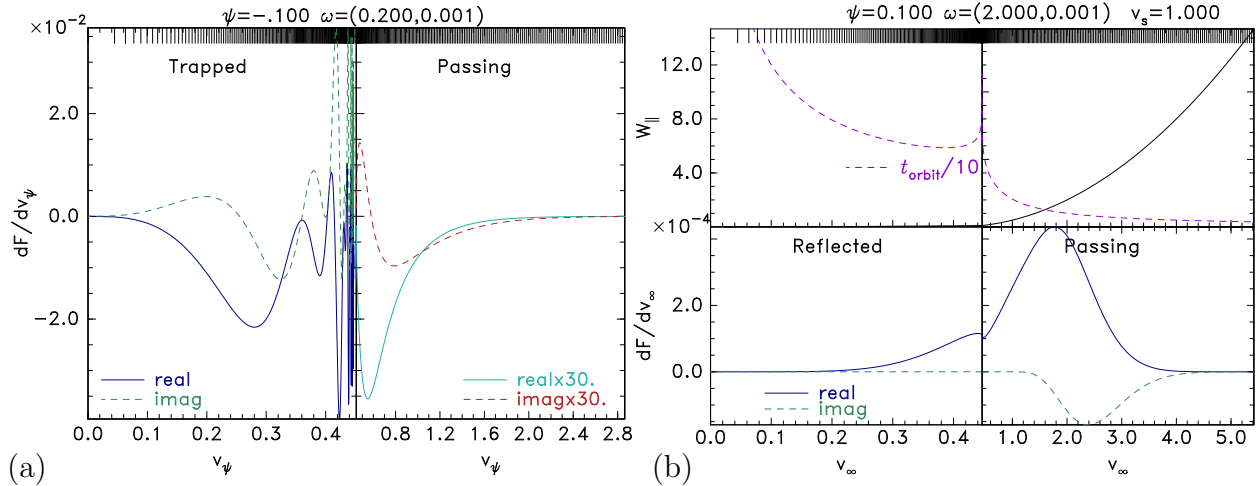


Figure 1: Illustration of the contributions to force dF/dv as a function of parallel velocity. (a) For the attracted species, as a function of v_ψ the velocity at the hole center $\phi = \psi$. Orbits are trapped for $v_\psi < \sqrt{2|\psi|}$. Note that passing force has been multiplied by 30 for visibility; so it is small. And its velocity axis scale is also different. (b) For the repelled species as a function of the distant velocity v_∞ , in which the upper panels show the energy and the orbit duration t_{orbit} . The non-uniform velocity integration mesh used is indicated at the top of each plot.

The background ion parallel velocity distribution is taken as the sum of two Maxwellian components of temperature T_i shifted by $\pm v_s$ and v_s will be stated in units of $\sqrt{T_i/m_i}$. Since ions are repelled by the hole, at some energies one must account for reflection of ions; and the contribution to force will then be different on the two sides of the hole if the ion distribution is asymmetric. Moreover an equilibrium will exist at only one hole velocity relative to the ion distribution [11, 18]. To avoid having to find the equilibrium, here only symmetric ion distributions $f_i(v)$ will be considered, for which the equilibrium hole velocity is $v_h = 0$ and the contributions from the two sides (two incoming ion velocities) to the perturbed \tilde{f}_i are equal.

The numerical calculation proceeds as follows. For a particular ω , the required maximum number of cyclotron harmonics is found, based on ζ_i ; then for each cyclotron harmonic m the integrals over z and equivalently τ of eq. (3), and then (6) or (8) are carried out numerically for fixed W_\parallel (and $dW_\parallel = v_z dv_z$ so that the phase-space element $dv_z dz \rightarrow dW_\parallel d\tau$). It proves more accurate to integrate eq. (3) as it stands, rather than first analytically integrating by parts as was previously done [14]. This improvement is especially important for the ion calculation, in which the frequency of interest is high relative to the bounce and transit frequencies. After multiplying $v_z dv_z \int \Phi_m dz$ by the terms $\omega_m \frac{\partial f_\parallel}{\partial W_\parallel}$ and $(\omega_m - \omega) f_\parallel$, the resulting dF , when divided by dv_z gives the differential contribution to force per unit v_z which is denoted $\frac{dF}{dv}$.

In Fig. 1 are shown illustrative cases of $\frac{dF}{dv}$ as a function of v_z , for $k = 0$ ($m = 0$). We observe that the *attracted* species force (a) is dominated by the trapped particles, the (single Maxwellian) passing contribution being practically negligible. Near the trapped-passing boundary ($W_\parallel = 0$ where $v_\psi = \sqrt{2\psi}$) oscillations require fine mesh spacing to resolve, but

their contribution is not strong because of the limited extent in v_ψ and significant cancellation. By contrast, the *repelled* species (b), normally ions, (whose plotted parameters are normalized to the ion thermal speed and plasma frequency) for which higher frequencies are dominant, has no such oscillations. However, its resolution challenges lie in the oscillations during integration of Φ_m on the spatial mesh, which are not visible in this plot. For this repelled species the time duration t_{orbit} of the orbit (to travel from and back to the chosen integration boundary) has a cusp at marginal reflection, and becomes very long for reflected orbits at lower energy, which dwell near reflection. The resulting averaging over fast ϕ_1 time-oscillations rapidly suppresses the perturbed force; and so passing orbit contributions dominate.

To get the total force for the entire velocity distribution, $\frac{dF}{dv}$ is multiplied by the $I_m(\zeta_t)$, and summed over relevant harmonics m . This process is mathematically equivalent to integrating over perpendicular distribution for low magnetic field, but for $\zeta_t \rightarrow 0$ requires only $m = 0$, the perpendicular Maxwellian integration having been transferred to the Bessel function. In this section and the next we show results only for this limit (effectively $k = 0$). We arrive at the total particle force \tilde{F} exerted by the potential, at this chosen ω . The complex ion force \tilde{F}_i as a function of real frequency (strictly for small positive imaginary part of ω) is plotted in Fig. 2, normalized to ψ^2 the hole potential amplitude squared, which is the dominant scaling. The tendency to a real constant value at high frequency is because

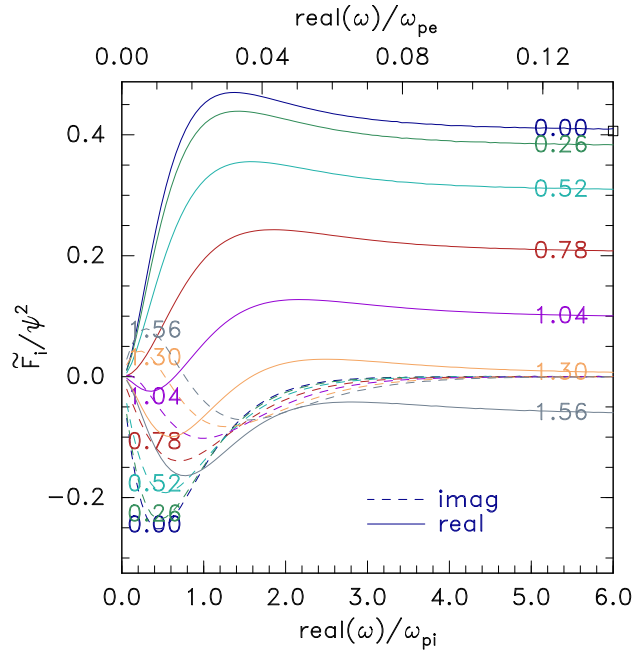


Figure 2: The real and imaginary parts of the ion force as a function of real ω for several different values of v_s labelling the curves. At high frequency, the force for an effectively immobile Maxwellian distribution $v_s = 0$ is shown by the square point, and agrees with the corresponding numerical integration line. The plot is independent of the value of hole amplitude ψ when it is small (0.001 here).

the ion charge density remains stationary when the potential shifts faster than the ions can

respond ($\omega \gg \omega_{pi}$). The reversal of the value with ion distribution shape (v_s) is because $f_{i\parallel}(v_z)$ develops a local minimum at $v = 0$ when the velocity shift of the components is more than ~ 1.1 . This is approximately the shape at which exponential instability ceases. A way to understand the force reversal intuitively is that the ion density in equilibrium becomes *larger* in the positive potential hole than outside it, rather than being smaller for a low shift (e.g. Maxwellian, $v_s = 0$). A positive equilibrium ion density deviation is repelled by the shifted potential, and the result tends to oppose the shift of the hole (recognizing that the hole has effectively negative inertia [16]). The algebra quantifies this intuition.

In Fig. 2, a square at the right hand side of the plot represents the analytic value $F_i = (128/315)\psi^2$ of the ion force for a small amplitude sech^4 shape hole and Maxwellian ions immobile on the timescale of the shift perturbation. Its agreement with the numerical calculation at $v_s = 0$ is one of the verification tests of the code. Another is that independent numerical calculation shows (reference [11] figure 2) that the immobile-ion force is zero for small ψ at $v_s = 1.3$, which is also in agreement with Fig. 2. Verification of the passing and trapped force code for the attracted species consists of a detailed quantitative comparison of the new code's force results with equivalent calculations from the independent prior code, whose results have been compared with analytic estimates [16] and PIC calculations [15], as well as agreement with the analytic electron force at very high frequency where even electrons are immobile ($\tilde{F}_e \rightarrow -(\frac{128}{35} - \frac{512}{63} + \frac{3200}{693})\psi^2 = -0.14776\psi^2$). There is an important adjustment in the electron force that arises, particularly for peaked ion distributions ($v_s \lesssim 0.5$). It is that the ion depletion contribution to the *equilibrium* charge changes the required equilibrium trapped electron depletion and thus changes $\frac{\partial f_{e\parallel 0}}{\partial W_{e\parallel}}$ for fixed $\phi(z)$. The effect is conveniently accounted for by scaling the electron depletion, i.e. the difference between the trapped distribution and a flat distribution $f_{e\parallel 0} - f_{e0}$ (eq. 11), by a single factor we shall write $1 + c_i$, where c_i is proportional to the ion equilibrium density non-uniformity, and is independent of W_{\parallel} . A fit to the ion response previously found [11] provides the value of c_i ¹. The factor $1 + c_i$ approximately doubles $f_{e\parallel 0} - f_{e0}$ at zero v_s , passes through unity near $v_s = 1.2$, and remains near 0.8 for higher v_s . This approximation of the ion equilibrium effects introduces uncertainties that are no greater than those implied by the adoption of the sech^4 potential form in the first place, and by the assumption that the eigenmode is the shiftmode.

The force-balance dispersion relation,

$$(\tilde{F} \equiv) \tilde{F}_e + \tilde{F}_i = F_E, \quad (12)$$

which is a complex equation requiring both real and imaginary parts to be zero, is not satisfied by an arbitrary complex ω . The ω that *does* satisfy it (if any), can be found either by contouring in the complex ω plane the real and imaginary parts of $\tilde{F} - F_E$ and finding where their zero contours cross, or by two-dimensional Newton iteration to find the complex root of $\tilde{F} - F_E$ (constrained by requiring $\text{Re}(\omega) \geq 0$ and $\text{Im}(\omega) \geq 0$).

¹The ad hoc fitting expression used is $c_i = [1 - (v_s/v_x)^\alpha]/[1 + \psi/4 + v_s\{v_s/[v_x + (3.3/v_s)^{1.5}]\}^\alpha]$, with $\alpha = 1.4$ and $v_x = 1.3 + 0.2\psi$

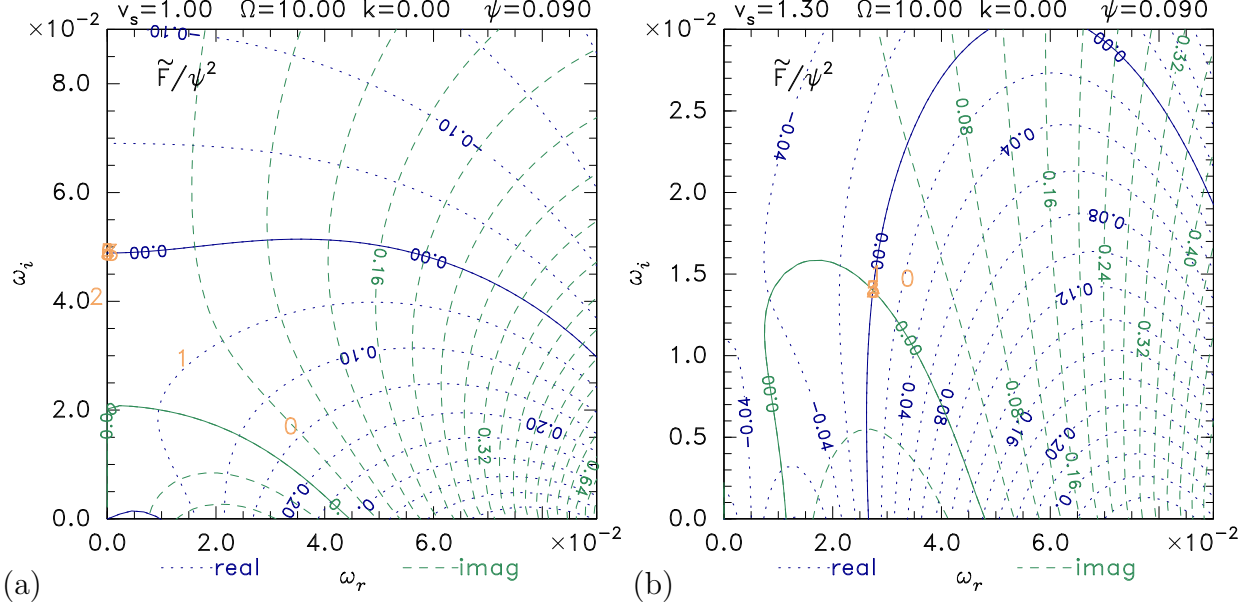


Figure 3: Contours of real and imaginary parts of total force \tilde{F} over the relevant complex ω region. Solid contours have value zero. The sequence of (orange) numbers on the plane show where Newton iterations (starting at 0) take the iterative solution. It converges at the intersection of the zero contours, where $\tilde{F} = 0$. In (a) $v_s = 1$ the solution lies on the $\text{Re}(\omega) = 0$ boundary, where $\text{Im}(\tilde{F}) = 0$. In (b) with larger ion component separation $v_s = 1.3$, there is no solution with $\text{Re}(\omega) = 0$, but a slower growing oscillation occurs at finite $\text{Re}(\omega)$.

3 One-dimensional Stability: Mechanism and Results

In this section we presume $k = 0$, which means $F_E = 0$ and motion is effectively one-dimensional. Figure 3 shows example contour plots of the total complex force in the complex ω plane. The complex root of the dispersion relation is where $\tilde{F} = 0$, at the intersection of the zero contours of its real and imaginary parts. At $v_s = 1$ (a), where there is no local minimum in the ion velocity distribution, a purely exponentially growing instability occurs at $\omega \simeq 0.05i$. At $v_s = 1.3$ (b), where a local minimum is present, the root is a slower-growing oscillation $\omega \simeq 0.028 + 0.014i$. This second type of solution was unaddressed in the prior slow hole stability analysis.

The disappearance of the purely growing mode can be understood by plotting the ion and electron forces along the $\text{Re}(\omega) = 0$ boundary. As shown in Fig. 4, although the ion force normalized to ψ^2 is very insensitive to the ψ -value, that is not true of the electron force. The reason is that F_e mostly comes from trapped particles whose bounce frequency is $\omega_b \propto \sqrt{\psi}$, and ω_b/ω determines the force variation. By contrast, the ion force is predominantly passing (no ion trapping), and has much weaker scaled dependence on ψ . When $v_s \gtrsim 1$ no intersection ($\tilde{F}_i = -\tilde{F}_e$) occurs for small enough ψ , and there is no instability having $\text{Re}(\omega) = 0$. All this is consistent with the previously published slow hole stability analysis concentrating on the high and negligible real frequency regions of the ω plane, which concluded that a local minimum in $f_i(v)$ was necessary for stability.

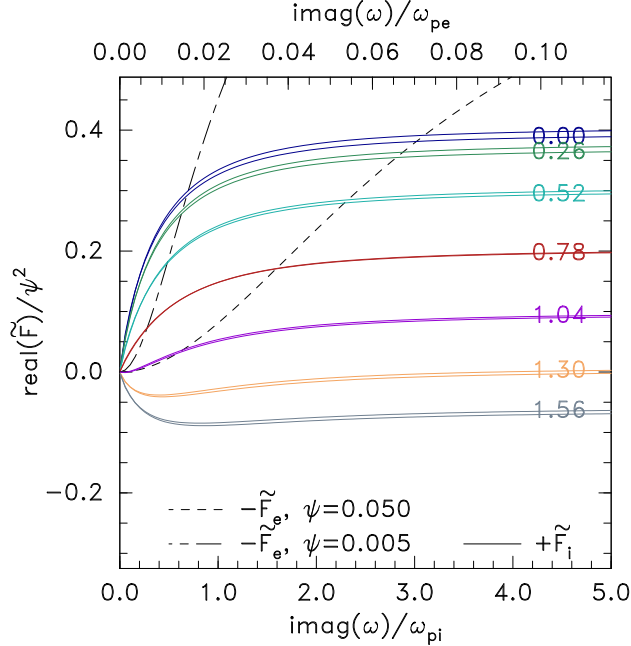


Figure 4: Scaled force \tilde{F}/ψ^2 as a function of purely imaginary ω . The ion force \tilde{F}_i is almost independent of ψ but depends on v_s shown by labels on the solid lines. The dashed curves give minus the electron force for the different ψ values. A growing mode requires $\tilde{F}_i = -\tilde{F}_e$: an intersection. When v_s is large enough, there are no intersections.

However, the *oscillatory* solution of Fig. 3(b) can remain even when there is a local f_i minimum if the $\text{Im}(\tilde{F}) = 0$ contour lies above the real ω -axis. The solution disappears if the hole amplitude is small enough, because the $\text{Im}(\tilde{F}) = 0$ contour disappears below the real axis, as Fig. 5 illustrates. The root itself, where $\text{Re}(\tilde{F}) = 0$ is zero as well as $\text{Im}(\tilde{F})$, likewise disappears. The case shown has just sufficiently low ψ for total stability. Newton iterations bump up against the $\text{Im}(\omega) \geq 0$ constraint without finding a zero. Decreasing ψ or increasing v_s moves the (barely visible) imaginary contour even further down out of the unstable domain.

Thus, there are really two requirements for the slow electron hole to be fully stable, to oscillatory as well as purely growing modes: (A) that there be a local minimum in the ion distribution $f_i(v)$ ($v_s \gtrsim 1.1v_{ti}$), and (B) that the hole's potential amplitude ψ should be small enough ($\psi \lesssim 0.01T_e/e$).

More quantitatively, a range of results is summarized in Fig. 6. At low v_s , the shift mode is purely growing, with a scaled rate $\text{Im}(\omega) \simeq 0.3\psi^{1/2}$ for a Maxwellian ($v_s = 0$) ion distribution. The transition to oscillation occurs close to $v_s = 1$, and the growth rate $\text{Im}(\omega)$ decreases quickly (as the local minimum of $f_i(v)$ develops) by a total factor of approximately 10. As that minimum deepens (v_s increasing further), the growth rate drops more slowly and the oscillation frequency $\text{Re}(\omega)$ increases until at a depth dependent on ψ the growth becomes zero and the instability disappears. If the amplitude is small enough $\psi \lesssim 0.01$, there is no oscillatory instability, and developing a local bare minimum in f_i is sufficient for stability.

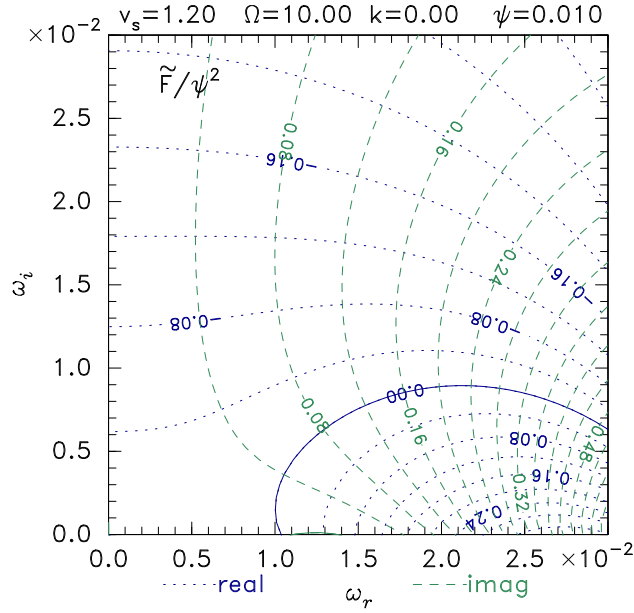


Figure 5: Force contours for a stable case at small ψ with sufficient ion component shift to give a local minimum. The negative imaginary contour is disappearing below the real axis removing the root of \tilde{F} from the unstable domain.

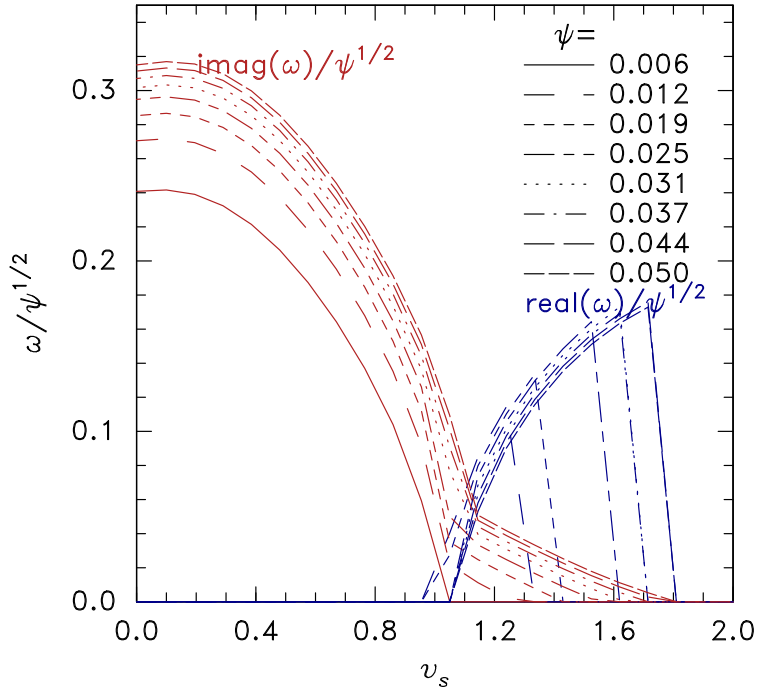


Figure 6: The real and imaginary parts of unstable mode frequency versus ion distribution shape (v_s), for a range of peak potential amplitudes (ψ).

4 Variation with other parameters

4.1 Ion Temperature

When ion temperature T_i is different from electron temperature ($= T_0$), the ion force is changed. Referring to equations 8 and 9, the quantities that are directly affected are $\frac{\partial f_{i\parallel 0}}{\partial W_{i\parallel}}$, $\frac{f_{i\parallel 0}}{T_{i\perp}}$, and ζ_{it} . In this subsection we will not address ζ_{it} changes with T_i . They give negligible effect in the strong ($\zeta_t \rightarrow 0$) and weak ($\zeta_t > 20$) magnetic field limits. For simplicity supposing the two parallel-shifted Maxwellian ion components remain isotropic, the effect of T_i changes on $\frac{\partial f_{i\parallel 0}}{\partial W_{i\parallel}}$ and $\frac{f_{i\parallel 0}}{T_{i\perp}}$ is to divide the ion force by T_i/T_0 ; because the changes arising from $f_{i\parallel 0}$ itself (reducing its height $\propto 1/\sqrt{T_i}$, and increasing its velocity width $\propto \sqrt{T_i}$), cancel each other out. Thus, the ion density perturbations, both in equilibrium and resulting from ϕ_1 , are multiplied by T_0/T_i . And since we are citing v_s in ion thermal units, the ion velocity distribution relative *shape* is independent of T_i . Therefore ion temperature can be accounted for by multiplying the ion force \tilde{F}_i and the equilibrium ion density non-uniformity by $1/T_i$.

Because the equilibrium ion density is changed by T_i , the electron force is also changed indirectly by adjustment of the required electron trapped distribution for equilibrium. The trapped electron equilibrium deficit is proportional to $(1 + c_i/T_i)$ and the electron force is scaled by the same factor, which varies more slowly than the ion force factor $1/T_i$.

Higher ion temperature therefore decreases the force on the ions relative to that on the electrons. Referring back to Fig. 4, the different scaling of these curves has the effect of moving the intersection $\tilde{F}_i = -\tilde{F}_e$ to lower imaginary values of frequency, that is of reducing the growth rate, as T_i increases.

Figure 7 illustrates the resulting variation of the instability frequency found by full numerical integration for $k = 0$. Increasing T_i always decreases the growth rate. For $v_s \lesssim 1.1$ the real frequency is zero, and is not plotted. For the oscillatory instability regime, $v_s \gtrsim 1.1$, increasing T_i can lead to a full stabilization: when $\psi = 0.05$ and $v_s = 1.5$ at $T_i \simeq 5$.

4.2 Transverse variation: Multidimensional Instability

Multidimensional instability here means situations in which although the equilibrium is independent of transverse position, the perturbation varies transversely: $k \neq 0$. And in this section we shall suppose that the magnetic field is strong enough that still only the $m = 0$ cyclotron harmonic matters because ζ_t remains small. In that case the only new effect is that the transverse Maxwell stress force F_E (eq. 7) is non-zero and must be included in the dispersion equation 12. Again suppressing the linear ξ factor, for the shift mode, it becomes

$$F_E = k^2 \int \left(\frac{d\phi_0}{dz} \right)^2 dz = k^2 \frac{128\psi^2}{315}, \quad (13)$$

where the final equality applies for the specific sech^4 potential shape. Therefore, if we consider the transverse wave-number k to be an arbitrary (real) choice, then we must examine the effect of including an F_E that is real and positive, but of arbitrary magnitude. Thus, we must allow the real part of \tilde{F} to be positive.

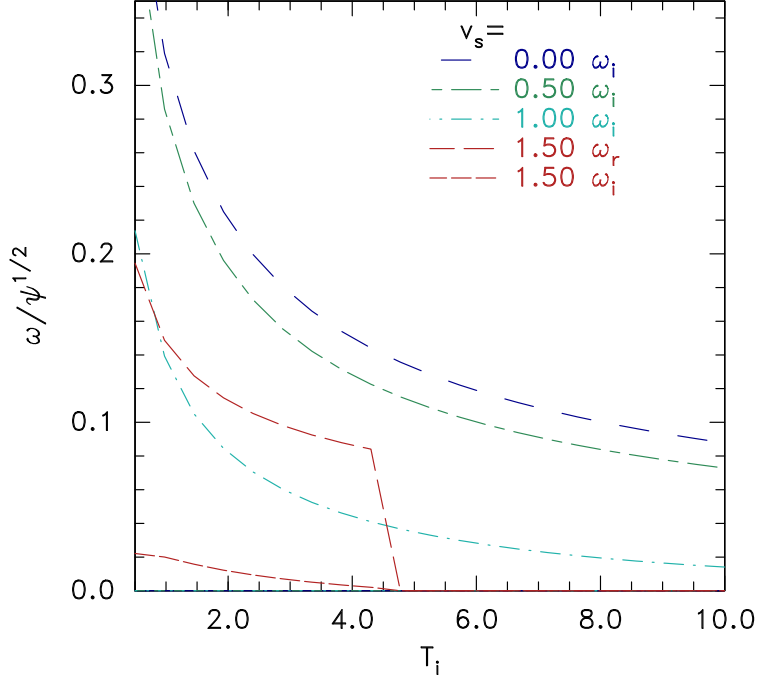


Figure 7: Variation of unstable frequencies (ω_i imaginary, ω_r real if non-zero) with ion temperature, for different v_s . $\psi = 0.05$.

The contour plots of Fig. 3 (for example) allow us immediately to deduce what happens to the unstable root as F_E increases from zero: it becomes the intersection of the unchanged solid $\text{Im}(\tilde{F}) = 0$ contour with a different real contour $\text{Re}(\tilde{F}) = F_E$, instead of zero. For example, in the case of Fig. 3(a) if a value $F_E = 0.1\psi^2$ is included, the relevant real contour is the one labelled 0.1. The root is then instead at $\omega \simeq (2.4 + 1.5i) \times 10^{-2}$, giving a slower growing oscillatory instability rather than the purely growing one for $k = 0$. By eq. 13 $F_E/\psi^2 = 0.1$ corresponds to $k = \sqrt{0.1 \times 315/128} = 0.496$, which is at the limit of high k , short wavelength; smaller k -values will have even less effect.

Similarly in Fig. 3(b) as k is increased, the relevant real contour moves to the right, and the root to higher real and lower imaginary frequency. For the case of Fig. 5, the motion of the real contour to the right can give the root a slightly positive imaginary frequency, and so induce a very slow instability where there was none before. But further increase of k brings the intersection past the region ($1.1 < \omega_r < 1.3$) where the imaginary contour is positive, thus restabilizing it.

To summarize, finite F_E arising from non-zero k *always* acts in such a direction as to make purely growing instabilities more stable, and *usually* does so even for oscillatory modes. We therefore do not spend further effort here to quantify in separate detail F_E -effects because almost always the $F_E = 0$ situation already treated is the most unstable. Nevertheless F_E is fully included in the results of the following section.

4.3 Magnetic Field Strength

When $k \neq 0$ and Ω is not very large, the Bessel function argument may not be small, and the sum over harmonics m may include many relevant terms. In this regime, the stability can depend on the magnetic field strength. Since the ion thermal Larmor radius r_L is greater than the electron by a factor $\sqrt{m_i/m_e}$ (for comparable temperature), the ions will generally experience $\zeta_t (= kr_L) \gtrsim 1$ first. The number of harmonics making significant contribution, when substantially greater than one, may be estimated by noting that $\zeta_t e^{-\zeta_t^2} I_m(\zeta_t^2)$, regarded as a function of integer m , is approximately a Gaussian $e^{-v_m^2/2}/\sqrt{2\pi}$, where $v_m = m/\zeta_t$. We therefore require contributions up to $v_m \sim 3$, i.e. $m \sim 3\zeta_t$. However with this velocity identification, $\omega_m = \omega + m\Omega = \omega + kv_m$, so writing $dv_m = 1/\zeta_t = \Omega/k$, eq. 9 becomes

$$\begin{aligned} & \sum_{m=-\infty}^{\infty} i \left[\omega_m \frac{\partial f_{\parallel 0}}{\partial W_{\parallel}} + (\omega_m - \omega) \frac{f_{\parallel 0}}{T_{\perp}} \right] q \Phi_m e^{-\zeta_t^2} I_m(\zeta_t^2) \simeq \\ & \sum_{m=-\infty}^{\infty} i \left[(\omega + kv_m) \frac{\partial f_{\parallel 0}}{\partial W_{\parallel}} + kv_m \frac{f_{\parallel 0}}{T_{\perp}} \right] q \Phi_0(\omega + kv_m) e^{-v_m^2/2} dv_m. \end{aligned} \quad (14)$$

The second form is a finite difference approximation of the unmagnetized integral expression: $\sum_{m=-\infty}^{\infty} dv_m \simeq \int_{-\infty}^{\infty} dv$. Thus, as physical considerations dictate, the limit of small Ω/kv_t gives simply an unmagnetized integral over the k -component of the perpendicular velocity distribution. This is often the case for the ions.

Although the numerical routine² evaluating the higher order Bessel functions (by backward recurrence) works well only up to approximately I_{60} , a maximum value of $|m| = 60$ is sufficient for the harmonic sum to represent the integral limit very well. It is then effectively already in the zero field limit. Therefore the present evaluation of \tilde{f} does not bother to switch to higher-resolution finite-difference integral representation, and instead artificially limits how small an Ω is permitted, and uses eq. 14 with an effective value of Ω no smaller than what requires a maximum $|m| \leq 60$, i.e. $\zeta_t \lesssim 20$. (The required effective Ω lower limit is different for electrons and ions.)

Figure 8 shows the effect of non-zero k and $\Omega = 2k$ on the cases of Fig. 3, with which it should be compared. Figure 8(a) and (b) have $k = 0.05$ and show mostly a movement of the contours downward toward more negative imaginary part (ω_i) of ω . (a) has a relatively small growth rate reduction; but (b), which has a local f_i minimum, shows complete stabilization of the prior unstable oscillatory mode. Figure 8(c) and (d) have the same ratio Ω/k as (a) and (b) but twice as large values: $k = 0.1$. In (c) the mode oscillates with real frequency $\omega_r \simeq 0.04$. In (d) there is again tendency to higher real frequency, compared with Fig. 3, but a very slow growing oscillatory instability remains, unlike (b) which was fully stabilized. The differences between (a) and (c) and between (b) and (d) are practically all differences in the electron force \tilde{F}_e , with a modest contribution from F_E differences. There is essentially negligible change in \tilde{F}_i , because ζ_t is so large that we are in regime of quasi-continuous perpendicular integration, and the value of kv_{ti} , much smaller than typical ω , gives little effect.

Figure 9 shows the real and imaginary parts of the dispersion solution ω as a function of magnetic field strength Ω . The different k values control the strength of the effect of

²RIBESL from the library TOMS715

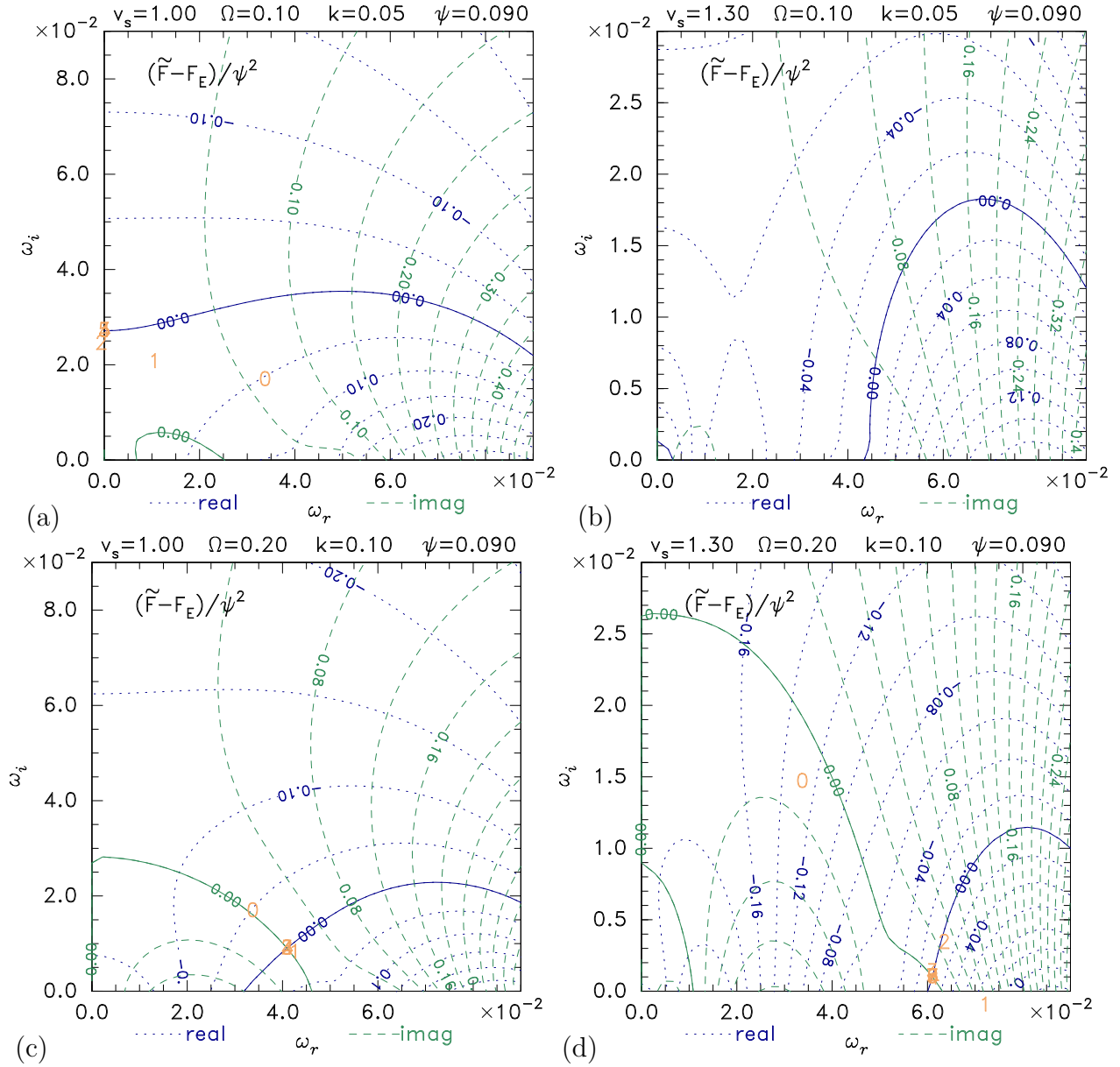


Figure 8: Force contours with non-zero k and low enough Ω to affect stability.

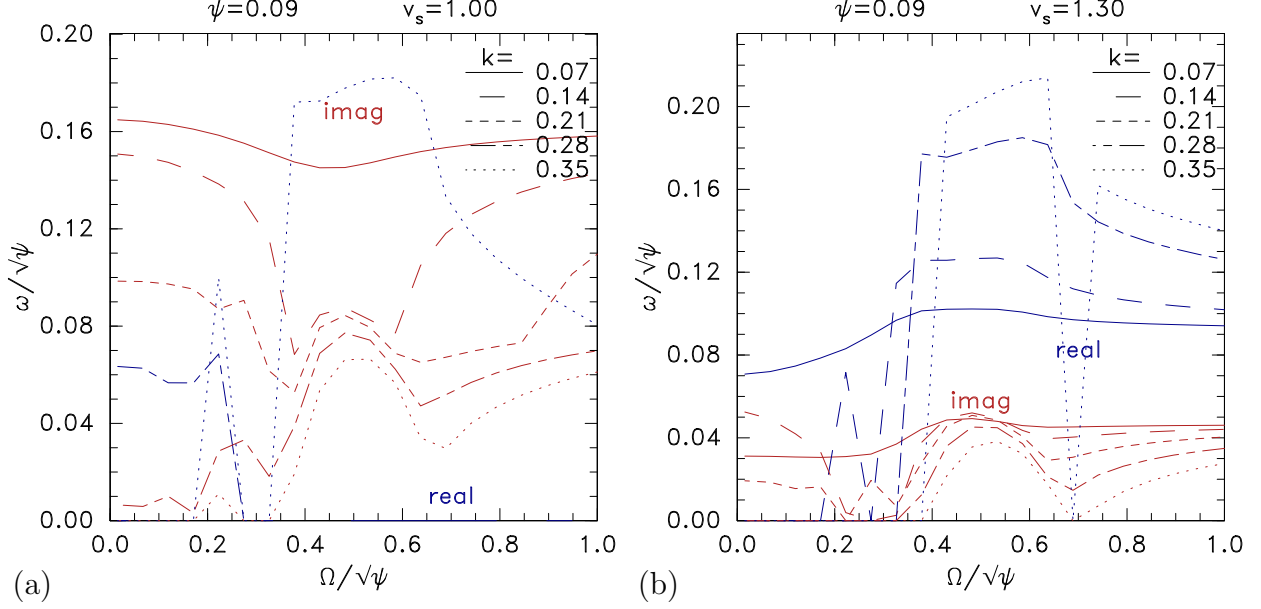


Figure 9: Dependence of the real and imaginary parts of the instability frequency on magnetic field strength, Ω , for a range of transverse wavenumbers k . (a) Single humped $f_i(v)$ $v_s = 1$; (b) double-humped $v_s = 1.3$, for a moderately deep hole $\psi = 0.09$.

transverse variation. The lowest $k = 0.07$ value (solid lines) shows rather weak variation from the $k = 0$ case (not shown) which gives a solution independent of Ω and equal to the high- Ω limit of the solid lines. In (a) the single-humped ion velocity distribution gives a purely growing mode ($\text{Re}(\omega) = 0$) at low k (0.07 and below) with growth rate approximately 0.16. All higher k values have growth rates smaller than this. Some of them make transitions to oscillatory ($\text{Re}(\omega) \neq 0$) modes in the middle of the Ω range, with growth rates typically half as great. In (b) for a double-humped ion distribution, similar trends are evident, but the growth rate is considerably smaller $\lesssim 0.05$, and the real frequency never reverts to zero at high Ω , consistent with the previous observation that for such distributions one-dimensional modes are all oscillatory, and are unstable at this ψ value.

At smaller potential amplitude, Fig. 10, the double humped $v_s = 1.3$ case (b) looks very different. It is stable for $\Omega/\sqrt{\psi} \gtrsim 0.65$ for all k values, consistent with Fig. 6. An oscillatory instability of low growth rate exists in the range $0.4 \lesssim \Omega/\sqrt{\psi} \lesssim 0.65$ except at very low k , and a purely growing mode below 0.4 for several k values. In fact this plot looks extremely similar to Figure 3 of [15], concerning transverse instability of *fast* electron holes with zero ion force. That is a sign that this instability is driven by the electrons with little contribution from the ions. It is effectively a slightly modified fast hole transverse instability. Fig. 10(a) with single humped ion distribution, by contrast, has unstable oscillatory solutions all the way out to large Ω . These are driven by the combined electron and ion response, and are limited to slow holes. The low Ω part of this plot has a character more like Fig. 10(a) than 9(b), and might be thought of as the transverse instability modified by the slow hole ion response.

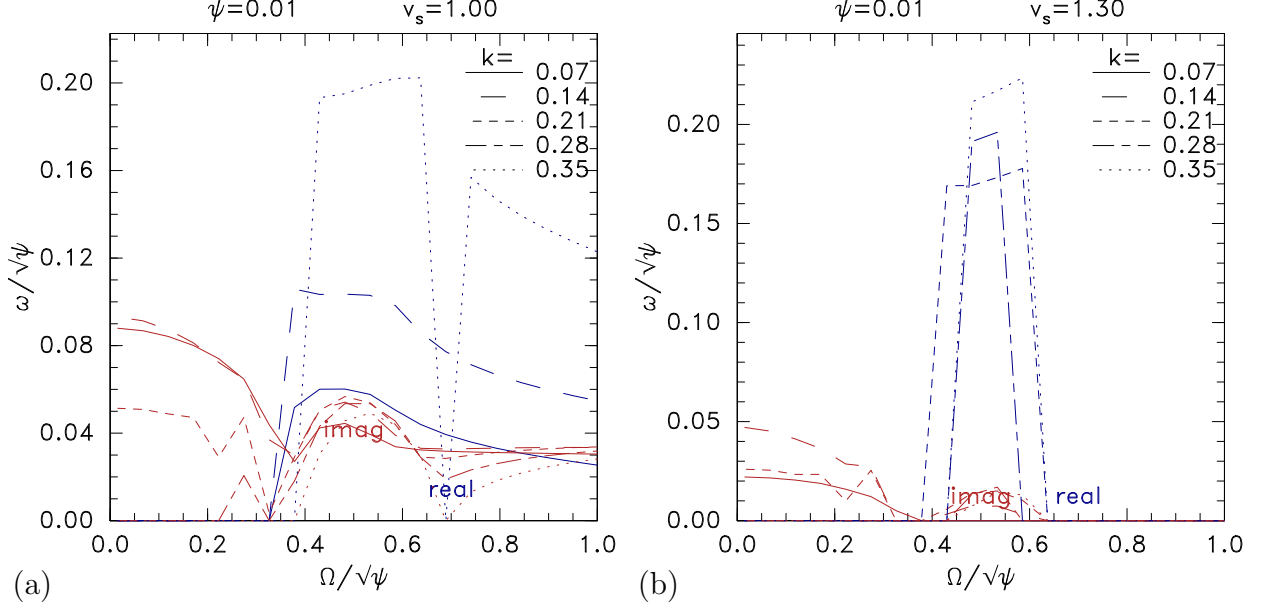


Figure 10: As in Fig. 9, except for smaller potential amplitude $\psi = 0.01$.

5 Summary

Slow electron holes are subject to instability of their velocity because of interaction with bulk ions. Purely growing one-dimensional ($k = 0$) instability disappears when a local minimum exists in the ion velocity distribution ($v_s \gtrsim 1.1v_{ti}$ for symmetric Maxwellian ion beams), in accordance with earlier studies. However, an oscillatory instability (overstability) remains up to relatively deep local minima, depending on the potential amplitude ψ of the equilibrium, as shown in Fig. 6. Its growth rate is much smaller than the purely growing mode. If the peak hole potential ψ is less than approximately $0.01T_e/e$ (for $T_i = T_e$ but larger for larger T_i see Fig. 7), the overstability disappears, this favors stability of *low amplitude* slow electron holes, which seems consistent with several observational studies [5].

When, $k \neq 0$, instabilities of slow holes have generally lower growth rate than when $k = 0$, except that when $(\Omega/\omega_{pe})/\sqrt{e\psi/T_e} \lesssim 0.6$ even low amplitude holes experience transverse instability driven predominantly by the electron response and not much affected by ion coupling. Its real frequency becomes zero if $(\Omega/\omega_{pe})/\sqrt{e\psi/T_e} \lesssim 0.4$.

An overall caveat to the present work is that it has analyzed only the pure shift mode. Under some circumstances a distorted shift can become more unstable [15]. This might modify the exact values of the instability thresholds.

The observational implications of the current results are broadly these. Slow electron holes in single humped background ion distributions will speed up without oscillations with growth time of order $0.3/(\psi^{1/2}\omega_{pe})$. They are predicted to remain slow for only a few growth times. By contrast, when f_i has a local minimum in which the hole speed lies, the oscillatory instability growth time is longer by of order a factor ten; so they remain slow at least that much longer, The oscillation real angular frequency is of order $0.1\psi^{1/2}\omega_{pe}$. When the hole potential is smaller or the f_i local minimum deeper, the growth rate of one-dimensional modes eventually becomes zero, unless the magnetic field is low enough that the electron

transverse instability is excited. Therefore the oscillatory instability discovered here can be avoided entirely in plausible parameter regimes. Furthermore, slow holes might be observed soon after formation even in regimes that have slowly growing instabilities.

It would be of considerable interest to verify by simulation the results of the present study. The required simulations for detailed quantitative comparison are rather difficult because they need a fully self-consistent steady slow hole initial equilibrium. My preliminary efforts, using hole potentials ψ considerably larger (0.2-0.4) than those for which this analysis predicts stability, do show oscillatory instabilities which are broadly consistent, being shift modes in approximately the right frequency range: $\text{Re}(\omega)/\psi^{1/2} \sim 0.1/\omega_{pe}$. However, the computational cost of simulations with sufficient signal-to-noise or velocity resolution increases rapidly with decreasing ψ , and have not yet been carried out in the lower- ψ stabilized regime.

Acknowledgements

I thank Ivan Vasko and his group for sharing their analysis of satellite data, which was a major impetus for this study. The work was not supported by any explicit funding. The codes that calculated the figures are publically available³.

References

- [1] I H Hutchinson. Electron holes in phase space: What they are and why they matter. *Physics of Plasmas*, 24(5):055601, may 2017. ISSN 10897674. doi: 10.1063/1.4976854. URL <http://aip.scitation.org/doi/10.1063/1.4976854>.
- [2] A. Lotekar, I. Y. Vasko, F. S. Mozer, I. Hutchinson, A. V. Artemyev, S. D. Bale, J. W. Bonnell, R. Ergun, B. Giles, Yu. V. Khotyaintsev, P.-A. Lindqvist, C. T. Russell, and R. Strangeway. Multisatellite mms analysis of electron holes in the earth’s magnetotail: Origin, properties, velocity gap, and transverse instability. *Journal of Geophysical Research: Space Physics*, 125(9):e2020JA028066, 2020. doi: 10.1029/2020JA028066. URL <https://agupubs.onlinelibrary.wiley.com/doi/abs/10.1029/2020JA028066>. e2020JA028066 10.1029/2020JA028066.
- [3] D B Graham, Yu V Khotyaintsev, A Vaivads, and M André. Electrostatic solitary waves and electrostatic waves at the magnetopause. *Journal of Geophysical Research: Space Physics*, 121:3069–3092, 2016. doi: 10.1002/2015JA021527.
- [4] K. Steinvall, Yu. V. Khotyaintsev, D. B. Graham, A. Vaivads, P.-A. Lindqvist, C. T. Russell, and J. L. Burch. Multispacecraft analysis of electron holes. *Geophysical Research Letters*, 46(1):55–63, 2019. doi: <https://doi.org/10.1029/2018GL080757>. URL <https://agupubs.onlinelibrary.wiley.com/doi/abs/10.1029/2018GL080757>.

³<https://github.com/ihutch/shiftmode>

- [5] Sergey R. Kamaletdinov, Ian H. Hutchinson, Ivan Y. Vasko, Anton V. Artemyev, Ajay Lotekar, and Forrest Mozer. Spacecraft observations and theoretical understanding of slow electron holes. *Phys. Rev. Lett.*, 127:165101, 2021. doi: 10.1103/PhysRevLett.127.165101. URL <https://journals.aps.org/prl/accepted/07072YbaR5a10a7219f86570217c2d7f68a24cecd>.
- [6] Koichi Saeki and J Juul Rasmussen. Stationary solution of coupled electron hole and ion soliton in a collisionless plasma. *Journal of the Physical Society of Japan*, 60(3): 735–738, 1991. ISSN 00319015.
- [7] L Muschietti, I Roth, R E Ergun, and C W Carlson. Analysis and simulation of BGK electron holes. *Nonlinear Processes in Geophysics*, 6(3/4):211–219, 1999. ISSN 10235809. doi: 10.5194/npg-6-211-1999. URL <http://www.nonlin-processes-geophys.net/6/211/1999/npg-6-211-1999.html>.
- [8] B Eliasson and P K Shukla. Dynamics of electron holes in an electron-oxygen plasma. *Physical Review Letters*, 93(4):45001, jul 2004. ISSN 0031-9007. doi: 10.1103/PhysRevLett.93.045001. URL <http://journals.aps.org/prl/abstract/10.1103/PhysRevLett.93.045001>.
- [9] B Eliasson and P K Shukla. Formation and dynamics of coherent structures involving phase-space vortices in plasmas. *Physics Reports*, 422(6):225–290, jan 2006. ISSN 03701573. doi: 10.1016/j.physrep.2005.10.003. URL <http://linkinghub.elsevier.com/retrieve/pii/S037015730500390X>.
- [10] C Zhou and I H Hutchinson. Plasma electron hole kinematics. II. Hole tracking Particle-In-Cell simulation. *Physics of Plasmas*, 23(8):82102, 2016. ISSN 10897674. doi: 10.1063/1.4959871. URL <http://dx.doi.org/10.1063/1.4959871>.
- [11] I. H. Hutchinson. How can slow plasma electron holes exist? *Phys. Rev. E*, 104: 015208, 2021. doi: 10.1103/PhysRevE.104.015208. URL <https://link.aps.org/doi/10.1103/PhysRevE.104.015208>.
- [12] Chuteng Zhou and Ian H Hutchinson. Plasma electron hole ion-acoustic instability. *J. Plasma Phys.*, 83:90580501, 2017. ISSN 0022-3778. doi: 10.1017/S0022377817000678.
- [13] Chuteng Zhou and Ian H. Hutchinson. Dynamics of a slow electron hole coupled to an ion-acoustic soliton. *Physics of Plasmas*, 25(8):082303, 2018. ISSN 1070-664X. doi: 10.1063/1.5033859. URL <http://aip.scitation.org/doi/10.1063/1.5033859>.
- [14] I H Hutchinson. Transverse instability of electron phase-space holes in multi-dimensional Maxwellian plasmas. *Journal of Plasma Physics*, 84:905840411, 2018. ISSN 0022-3778. doi: 10.1017/S0022377818000909. URL <http://arxiv.org/abs/1804.08594>.
- [15] I. H. Hutchinson. Transverse instability magnetic field thresholds of electron phase-space holes. *Physical Review E*, 99:053209, 2019. doi: 10.1103/PhysRevE.99.053209.

- [16] I H Hutchinson. Electron phase-space hole transverse instability at high magnetic field. *Journal of Plasma Physics*, 85(5):905850501, 2019. ISSN 14697807. doi: 10.1017/s0022377819000564.
- [17] B. N. Parlett. The Rayleigh Quotient Iteration and Some Generalizations for Nonnormal Matrices. *Mathematics of Computation*, 28(127):679–693, 1974. ISSN 00255718. doi: 10.2307/2005689.
- [18] I. H. Hutchinson. Asymmetric one-dimensional slow electron holes. *Phys. Rev. E*, 104:055207, Nov 2021. doi: 10.1103/PhysRevE.104.055207. URL <https://link.aps.org/doi/10.1103/PhysRevE.104.055207>.